

# SMART-1 MOON IMPACT OPERATIONS

A. Ayala<sup>(1)</sup>, R. Rigger<sup>(2)</sup>

<sup>(1)</sup>ESOC GMV, Robert-Bosch-Str. 5, D-64293 Darmstadt, Germany, E-mail: [Andres.Ayala@esa.int](mailto:Andres.Ayala@esa.int)

<sup>(2)</sup>ESOC EDS, Robert-Bosch-Str. 5, D-64293 Darmstadt, Germany, E-mail: [Ralf.Rigger@esa.int](mailto:Ralf.Rigger@esa.int)

## 1. ABSTRACT

This paper describes the operations to control the Moon impact of the 3-axis stabilized spacecraft SMART-1 in September 2006.

SMART-1 was launched on 27/09/2003. It was the first ESA mission to use an Electric Propulsion (EP) engine as the main motor to spiral out of the Earth gravity field and reach a scientific moon orbit [1]. During September 2005 the last EP manoeuvres were performed using the remaining Xenon, in order to compensate for the 3<sup>rd</sup> body perturbations of the Sun and Earth. These operations extended the mission for an additional year. Afterwards the EP performance became unpredictable and low, so that no meaningful operation for the moon impact could be done. To move the predicted impact point on the 16/8/2006 into visibility from Earth an alternative Delta-V strategy was designed. Due to their alignment, the attitude thrusters could not be used directly to generate the Delta-V, so this strategy was based on controlled angular momentum biasing. Firing along the velocity vector around apolune, the remaining Hydrazine left from the attitude control budget was used, to shift the impact to the required coordinates.

## 2. INTRODUCTION

The SMART-1 AOCS allows the S/C to follow any attitude profile commanded by the ground. The attitude control is based on reaction wheels as actuators for all

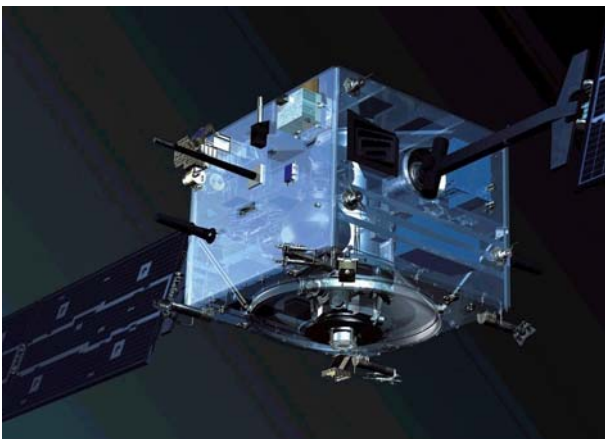


**Fig. 1:** SMART-1 with attitude thruster pairs at the bottom. Illustration by AOES Medialab, ESA 2002.

nominal modes and 1N attitude (Hydrazine) thrusters for reaction wheel desaturation and for rate reduction in case of contingencies. These 2x4 attitude thrusters are mounted along the Z-axis away from the centre of mass, pointing in the X/Y-plane of the S/C. This means that Delta-V ( $\Delta V$ ) and Delta-L ( $\Delta L$ , where L is the S/C total angular momentum) can occur simultaneously. Two autonomous star trackers, 5 attitude rate sensors (gyroscopes) and 3 coarse sun sensors are utilized as attitude sensors.

The EP engine is mounted on a two axes articulation mechanism (EPMEC) attached to the S/C. While the engine is firing, a control loop of the AOCS aims to reduce the total S/C angular momentum by rotating the EP engine with respect to the S/C-body. The control loop reaches a steady state when the EPMEC-articulation is such that the thrust direction points to the S/C centre of mass. In this steady state, the thrust direction is about 4 degrees away from its mid-position, in which the thrust vector is aligned with the S/C Z-axis. Typical excursions from the steady state rotation angles are of the order of 1 degree. As a result of this momentum management with the EP thrust, which worked better than expected, the Hydrazine budget was not exhausted, so that approximately 6 kg of Hydrazine were left, and could be used for the required  $\Delta V$  at the end of the mission.

The solar arrays (SA) are mounted along the S/C Y-axis, and can be rotated infinitely. The Star Trackers (ST) are mounted on the +/-Y-faces with their boresights about 40 degrees away from the +/-Y-axis. Therefore, the Sun will never be in the field of view (FOV) of a ST as long as the SA panels are perpendicular to the Sun direction (S). However, it is possible for a ST to be blinded by the Earth or the Moon. Simultaneous blinding of both STs must be avoided, since the attitude rate sensors do not permit the outage of both STs for more than one hour. This was especially delicate at times when the S/C was at low moon altitude. Apart from constraining the attitude, the STs also impose a constraint on the S/C rate: To guarantee proper tracking the angular S/C rate was qualified to 0.15 degrees/s [2]. Due to a limitation in the torque that can be exerted on the reaction wheels, the angular acceleration of the S/C was qualified to 0.0005 degree/s<sup>2</sup>.

## 2.1 Initial situation

The scientific community requested the impact point over the Moon's terminator, with the best illumination conditions for impact observation. This request was driven by various scientific objectives. Namely spectrometric information constraining the mineralogy, the thermal and dynamic evolution of the impact flash and the ejecta morphology [3].

After about 2 years in operation, SMART-1 reached the operational Moon orbit in early 2005. Six months later in September 2005 a further series of EP manoeuvres were performed to extend the mission. These manoeuvres were symmetric to the perilune, so the line of apsides is rotated to a point where the Earth and Sun perturbations initially raise the perilune again.

To extend the operational period to a maximum the second extension took into account that the Xenon was exhausting. Therefore, the strategy for the last firing period of the EP had to consider that it could be stopped at any time. In the end, almost all of the second firing was performed and from this time on the engine was declared no longer reliable (and operation was stopped). This left SMART-1 in a free drift orbit from where the S/C would eventually crash into the Moon, due to the increasing eccentricity. In fact the orbit propagation predicted (for this free drift orbit), that the security height of 300 km would be violated on the 8th June 2006 and the S/C would crash on the 17th August 2006. However since the prediction period was almost one year, these results had an error in the impact time of more than a day due to the fact that irregularities of the Moon's surface were not precisely known.

The first part of the paper describes how the Delta-V was implemented using the four attitude thrusters, the

pointing profiles [4] required and the S/C dynamics involved [5]. The second part shows how the manoeuvres were calculated and optimised to achieve the scientific requirements of the impact.

## 3. IMPLEMENTATION OF THE DELTA-V

### 3.1 Chosen strategy

To implement the required  $\Delta V$ , the following idea for the usage of the attitude thrusters was chosen: Command alternating target angular momentum along the symmetry axis of the solar arrays, i.e. the y-axis of the S/C, with synchronically alternating attitude around the same axis. The parameters sent to the S/C are the target levels of the wheels. Since the attitude thrusters are asymmetric about the S/C centre of mass, this will lead to a  $\Delta V$ , which can be used to adjust the orbit [Fig. 2] and [Fig. 3].

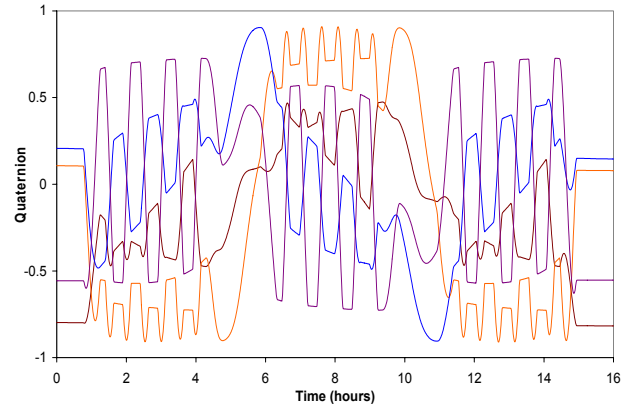


**Fig. 3:** Commanded quaternion profile: Apart from rotating the body, adjustments for the pointing direction and the constraint of sun aspect angle (to 90 degrees) are made [4]

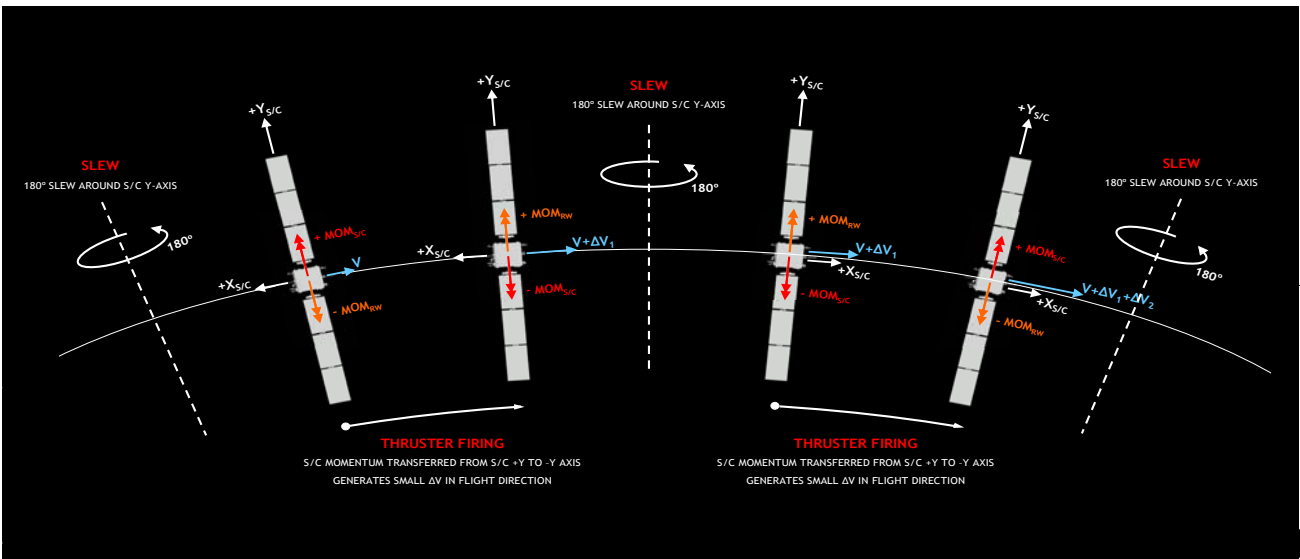


**Fig. 2:** Chosen strategy: To achieve the required Delta-V seven Delta-L manoeuvres per orbit are made with re-orientation of the S/C body and therefore the thrusters in-between [6]

This option was preferred amongst others, since the S/C had many constraints, the efficiency was high, the required performance could be reached and the dynamics was controllable.

### 3.2 RCS model and AOCS controller

Each Delta-L will linearly translate into a Delta-V:

$$\Delta V_{WoL} = M_{Force} \cdot M_{Torque}^{-1} \Delta L$$

since  $\Delta V_{WoL} = M_{Force} T_{on}$  and  $\Delta L = M_{Torque} T_{on}$ ,

where  $M_{Force}$ ,  $M_{Torque}^{-1}$  and  $T_{on}$  are the force matrix, the pseudo inverse of the torque matrix and the thruster on-times respectively.

Apart from compensation for the accumulated disturbance torques, the first  $\Delta L$  will load 2 Nms along the Y-axis. Each subsequent  $\Delta L$  (of 4 Nms) will flip this to -2 Nms along the same axis. Finally, a last  $\Delta L$  will bring the total S/C angular momentum back to zero. Therefore, the resulting  $\Delta V$  in the S/C frame will also alter in-between +/- 0.0264 m/s (or half of that) along the X-axis. The geometry of the three torque controlled reaction wheels, is such that one of them will only be used for the compensation of the attitude and external disturbances.

Finally flipping the S/C body around the Y-axis by 180 degrees after each  $\Delta L$ , will cause the  $\Delta V_{WoL}$  in the inertial frame to accumulate in the required direction [Fig. 4]. These flips have two advantages: rotations take place around the smallest moment of inertia of the S/C and the rotations can be chosen such that the loaded angular momentum will temporarily decrease during

each slew [Fig. 4], so that no extra margins or constraints occur.

Using the techniques as described in [4] and applying an improved slew (with the difference that the angular velocity is now split in three phases: acceleration, coast arc and deceleration [Fig. 4]) these manoeuvres can be performed fulfilling all S/C operational constraints, namely keeping the SA panels perpendicular to the Sun. However, since the resulting  $\Delta V_{WoL}$  appeared too small, there were several options considered to improve this situation:

- Usage of all four reaction wheels. This would allow to load twice as much  $\Delta L$ .
- Shorten the time for the slews by violating the rate constraint.
- Speed up the duration of the  $\Delta L$  by adjusting the duty cycle.

After an investigation from ESOC/FD and SSC [5] option 2 was chosen, such that the maximal S/C rate was 0.23 degrees/second, since the limiting factors the controller of the SA mechanism and the Star Trackers proved to be able to cope with this rate. The angular acceleration of the S/C was set to 0.00375 degree/s<sup>2</sup>, well within the values of [5], but above initial qualification. This was possible due to the very solid AOCS controller of SMART-1 and relatively low pointing accuracy requirements. It means that all standard operational constraints were fulfilled with the exception of the rate and torque limit during the very fast 3-segment slews. However, some operational obstacles like cat bed (thruster) heating [5] and communication were also adjusted in order to cope with this strategy.

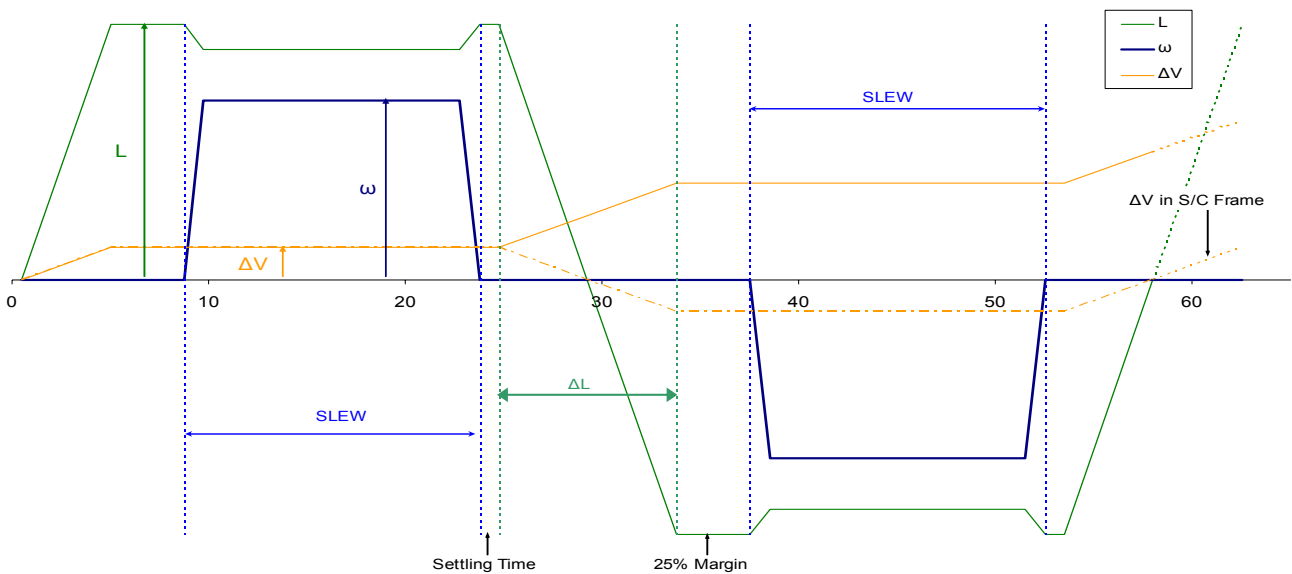


**Fig. 4:** Evolution of the angular momentum (L) in S/C frame along the Y-axis of the S/C, the angular velocity (w) and the resulting accumulated velocity increment ( $\Delta V$ ) along the required thrust direction over time (in minutes).

### 3.3 Global attitude

As described below the  $\Delta V_{wol}$  was performed around apocentre. During each orbit 7 off-loads of the angular momentum to  $\pm 2$  Nms along the S/C y-axis, and one extra off-load for each perilune (to compensate external torques) were performed. The perilune passage was commanded to be done Nadir pointing of the Z-axis to minimize the gravity gradient torque. Several Earth communication blocks were also inserted. The standard command generation software for the attitude and  $\Delta L$  could be used. Only the interface with the optimisation software was adjusted to simulate a standard thruster behaviour. Starting on the 19/6/2006, overall more than 520 reaction wheel off-loads were executed during the first campaign. Later during a second campaign another 21  $\Delta L$  manoeuvres were executed.

### 3.4 Performance

The uncertainty in the off-load target was expected to be the largest error source due to the size of the off-load target threshold. However, over many off-loads these uncertainties averaged out as expected, resulting in only about 0.5-1% overall misperformance. The RCS modelling was supported by orbit determination and the respective performance calibrations. Further, the propagation of the reaction wheel was based on calibrated data from prior telemetry. The central problem was the estimate of the duration of an off-load. Since for performance reasons each slew needed to start as close as possible to the end of a  $\Delta L$  manoeuvre, but still ensuring the finalization of the  $\Delta L$  before this time, a 25% margin was assumed. A total  $\Delta V$  of 11.8 m/s using 2.5 kg Hydrazine to raise the pericentre by 90 km in total was performed

## 4. FULL OPTIMISATION SCHEME

The objective of the optimisation was not to extend the mission or save up Hydrazine. The target was to reach height 0 for the first time in a point visible from the Earth and observable by the ground stations.

Based on the small  $\Delta V_{wol}$  manoeuvres available, the optimisation strategy was to perform these in groups (of G, typically 5 or 7) distributed symmetrically with respect to the apolune (positioning them by true anomaly). Each such  $\Delta V_{wol}$  had the same magnitude and was pointing along the S/C velocity direction. For every orbit with manoeuvres, this would give an equal total impulse:

$$\Delta V_{orb} = G \cdot \Delta V_{wol}$$

To gain enough degrees of freedom two of such series were planned one for end of June and one in July with a coast phase between them. A third slot in August was reserved for corrections.

This full optimisation problem was solved numerically with MANTRA, an operational manoeuvre optimisation and trajectory propagation software tool. The most important perturbations considered are:

- 3<sup>rd</sup> Body, specially Earth and Sun
- Moon W91 gravity field, up to 20x20 terms.
- Solar radiation pressure and eclipse effect
- Moon surface model W91 with a resolution of 0.25 degrees in longitude and latitude.

This approach had two main difficulties. It is heavily time consuming due to the high accuracy required for the long-term propagation. Further, the number of manoeuvres per orbit (G) and number of orbits per series (N) are discrete parameters that were input to the software package. These parameters must therefore be determined before hand manually:

## 5. LINEAR APPROXIMATION

The complete optimisation problem required an approximation, which allowed fast generation of the initial conditions, i.e. the numbers G and N. This was also of vital importance during operations to be able to generate the results on time.

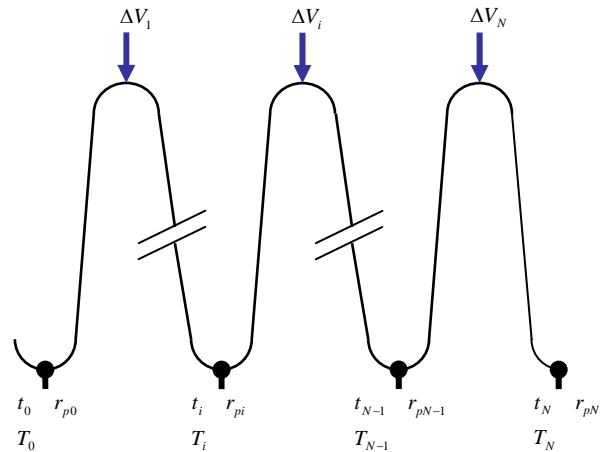


Fig. 5: Manoeuvre scheme

### 5.1 Fundamental idea

The low magnitude of the manoeuvres allowed assuming, that the effect of each is linear and independent of the previous one. So, a straightforward practical solution to the complete problem is to model it

as a superposition of single firings. The manoeuvres around the apolune are considered equivalent to a single instantaneous manoeuvre at the apolune [Fig. 5]. In addition, the effect of the impulse at each apolune is independent of the previous one. Firing along the velocity direction the Gauss perturbation equations [8] show that only the in-plane parameters semi major axis (a) and eccentricity (e) -or equivalent the orbital period and perilune radius- will be affected.

The change in these parameters is therefore modelled to be linear in the  $\Delta V$  magnitude and for a succession of i apolunes (with manoeuvre) the approximation becomes:

$$\begin{aligned} r_{pi} &\approx r_{p0} + i \cdot K_1 \cdot \Delta V \\ T_i &\approx T_0 + i \cdot K_2 \cdot \Delta V \end{aligned} ,$$

where  $r_{pi}$  is the perilune radius and  $T_i$  the orbit period of the i-th orbit.  $K_1$  and  $K_2$  are proportional constants, related to the physics of the problem.

For N orbits, the approximation of the orbital period can be used to estimate the final time (taking into account that the first and last orbits count only half):

$$\begin{aligned} t_f &= t_0 + \frac{T_0}{2} + \sum_{i=1}^N T_i - \frac{T_N}{2} \\ &= t_0 + N \cdot T_0 + \frac{N^2}{2} \cdot K_2 \cdot \Delta V \end{aligned} ,$$

where the following expressions were taken into account:

$$\begin{aligned} \frac{T_0}{2} - \frac{T_N}{2} &= -\frac{N \cdot K_2 \cdot \Delta V}{2} \\ \sum_{i=1}^N T_i &= N \cdot T_0 + K_2 \cdot \Delta V \cdot \sum_{i=1}^N i \\ \sum_{i=1}^N i &= \frac{N \cdot (N+1)}{2} \end{aligned} .$$

## 5.2 Perturbation equation

In an intermediate step, we use the perturbation equations to prepare the deduction of a more rigorous estimate in the next section.

As the firing is tangential to the orbit, no out-of-plane parameter (inclination, line of nodes) is affected.

It is known that the time derivatives of the semi major axis a, the eccentricity e and the argument of perilune  $\omega$  for a tangential manoeuvre at the moon apocentre ( $\nu = \pi$ ) are:

$$\begin{aligned} \frac{da}{dt} &= \frac{2 \cdot a^2 \cdot V}{\mu} \cdot \gamma = \frac{2 \cdot a^2 \cdot V_a^2}{\mu} \cdot \frac{\gamma}{V_a} \\ \frac{de}{dt} &= \frac{2 \cdot (e + \cos(\nu))}{V} \cdot \gamma = 2 \cdot (e - 1) \cdot \frac{\gamma}{V_a} \\ \frac{d\omega}{dt} &= \frac{2 \cdot \sin(\nu)}{e \cdot V} \cdot \gamma = 0 \end{aligned} .$$

Here V is the velocity of the S/C,  $\mu$  the gravitational parameter of the moon,  $\nu$  the true anomaly and  $\gamma$  the applied acceleration along the velocity.

The third equation shows that the argument of perilune does not change for a manoeuvre at apolune. The Earth-Sun perturbation keeps its value, and it is only changed by a small amount, resulting from the Earth and Moon movement. For the velocity in the apolune we have

$$V_a = \sqrt{\frac{\mu}{p} \cdot (1 - e^2)} .$$

Putting all together with the definition of the semilatus rectum,  $p = a \cdot (1 - e^2)$  we get for instantaneous increments

$$\begin{aligned} \frac{\Delta a}{a} &= 2 \cdot \frac{1 - e}{1 + e} \cdot \frac{\Delta V}{V_a} \\ \Delta e &= -2 \cdot (1 - e) \cdot \frac{\Delta V}{V_a} \end{aligned} ,$$

by using the variables  $\lambda$  and  $\varepsilon$  i.e.

$$\lambda = \frac{r_p}{r_a} = \frac{1 - e}{1 + e}, \quad \varepsilon = \frac{\Delta V}{V_a}$$

the above equations become

$$\begin{aligned} \frac{\Delta a}{a} &= 2 \cdot \lambda \cdot \varepsilon \\ \frac{\Delta \lambda}{\lambda} &= 2 \cdot (1 + \lambda) \cdot \varepsilon \end{aligned} .$$

As T is the osculating orbital period, then we get from the 2<sup>nd</sup> Kepler law

$$\frac{\Delta T}{T} = \frac{3}{2} \cdot \frac{\Delta a}{a} = 2 \cdot \lambda \cdot \varepsilon .$$

Therefore, the derivative of the radius of the perilune fulfils

$$\left. \begin{array}{l} r_p = r_a \cdot \lambda \\ r_a = const \end{array} \right\} \Rightarrow \frac{\Delta r_p}{r_p} = \frac{\Delta \lambda}{\lambda} = 2 \cdot (1 + \lambda) \cdot \varepsilon$$

With these results, we can now determine the radius of the perilune and the period in each perilune.

### 5.3 Constants and error estimation

Here we give a quantitative estimate of the intuitive linearization idea from 5.1.

First, the problem can be simplified by assuming that the increment in apolune velocity  $\Delta V_{orb}$  is small (of the order of  $1 \text{ cm/s}$ ) relative to the overall velocity at apolune  $V_a$  (of the order of  $1 \text{ km/s}$ ), i.e.

$$\varepsilon_0 = \frac{\Delta V}{V_{a0}} \approx \frac{1 \text{ cm/s}}{1 \text{ km/s}} = 10^{-5}$$

So the next approximations will keep only terms of the order of  $\varepsilon_0$ . Second, the increase of  $\varepsilon$  due to the variation in the apolune velocity is small:

$$\left. \begin{array}{l} V_{a_i} = V_{a_0} + i \cdot \Delta V_{orb} \\ \varepsilon_i = \frac{\Delta V_{orb}}{V_{a_0} + i \cdot \Delta V_{orb}} = \frac{\varepsilon_0}{1 + i \cdot \varepsilon_0} \end{array} \right\} \Rightarrow \varepsilon_i \cong \varepsilon_0 = \frac{\Delta V_{orb}}{V_{a_0}}$$

That limits the number of manoeuvres to be much smaller than  $1/\varepsilon_0 = 10^5$ , and allows an easier comparison of terms with  $\varepsilon$ , since  $\varepsilon_i$  and  $\varepsilon_0$  are of the order of  $10^{-5}$  (of course depending on the magnitude of  $i$ )

The next simplification is to keep the right hand term of the equations constant (see 5.2). To see how restrictive the number of orbits actually is, we study the evolution of the parameter  $\lambda$  using the full expression (but applying simplification of  $\varepsilon_i$ ) and the simplified one:

$$\begin{aligned} \lambda_i &= \lambda_{i-1} + 2 \cdot \varepsilon \cdot \lambda_{i-1} \cdot (1 + \lambda_{i-1}) \\ \tilde{\lambda}_i &= \tilde{\lambda}_{i-1} + 2 \cdot \varepsilon \cdot \lambda_0 \cdot (1 + \lambda_0) \end{aligned}$$

The SMART-1 orbit had a high eccentricity with a typical value of 0.4 or higher. This results in a range for  $\lambda$  of  $0.3 < \lambda < 0.5$ .

The graph [Fig. 6] shows the divergence between both series. The difference is lower than  $\varepsilon_0$  while  $N < 200$  for the range of initial values considered, giving a tight limit for the number of manoeuvres. For bigger values,

the error becomes greater or equal to  $\varepsilon_0$ . In this case, the error becomes of the magnitude of  $\Delta V_{orb}$ .

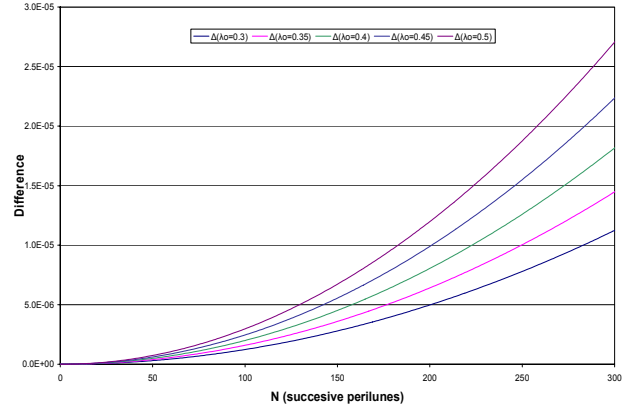


**Fig. 6:** Plot of  $\lambda - \tilde{\lambda}$  for several initial values of  $\lambda$  and a value of  $\varepsilon_0 = 10^{-5}$

With this the expressions for the perilune radius and the period after the  $i$ -th manoeuvre are

$$\begin{aligned} r_{p_i} &= r_{p_0} \cdot (1 + 2 \cdot (1 + \lambda_0) \cdot \varepsilon)^i \\ T_i &= T_0 \cdot (1 + 3 \cdot \lambda_0 \cdot \varepsilon)^i \end{aligned}$$

Using the approximation,  $(1 + x)^n = 1 + n \cdot x + o(x^2)$  we can rewrite the previous equations as

$$\begin{aligned} r_{p_i} &\approx r_{p_0} + 2 \cdot i \cdot (1 + \lambda_0) \cdot \varepsilon \\ T_i &\approx T_0 + 3 \cdot i \cdot \lambda_0 \cdot \varepsilon \end{aligned}$$

These last expressions are again a linear approximation of the perilune and period as a function of the impulse. Moreover, a comparison with results from chapter 5.1 shows:

$$K_1 = 2 \cdot \frac{1 + \lambda_0}{V_{a0}}, \quad K_2 = 3 \cdot \frac{\lambda_0}{V_{a0}}$$

So now, we see that for a series of less than 200 manoeuvres our approximation has an error of the magnitude of  $\Delta V_{orb}$ .

## 6. FURTHER CONSIDERATIONS

### 6.1 Decay of the perilune

With these results being valid for each manoeuvre series a model of the overall scheme is obtained. The plot of the osculating radius of the perilune at perilune as function of time allows us to obtain two powerful results.

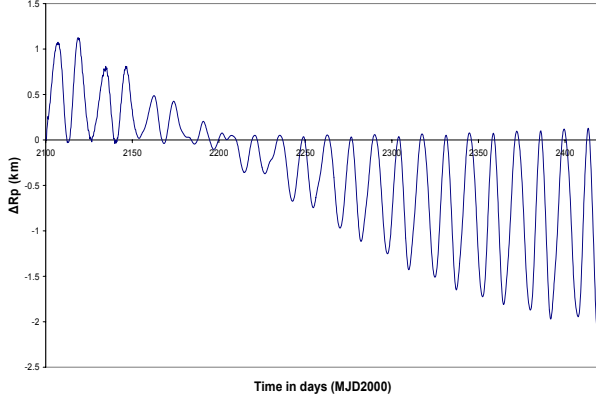


**Fig. 7:** Perilune change per revolution up to SMART-1 impact (without manoeuvres).

First and most important is that during the impact period the change in perilune radius must be strictly negative [Fig. 7]. This will guarantee that the impact cannot be delayed by this effect, i.e. will happen in a near by orbit (max 5.5 hours error)

The second result is that for long coast periods the decay of perilune can be approximated by its mean value (D)

We can combine the results (using the sub index  $\alpha$  for the parameters of the first series,  $\beta$  for the second series and L for the number of coast orbits)

$$\begin{aligned}\Delta r_\alpha &= N_\alpha \cdot K_\alpha \cdot \Delta V_\alpha - D_\alpha \cdot L_\alpha \\ \Delta r_\beta &= N_\beta \cdot K_\beta \cdot \Delta V_\beta - D_\beta \cdot L_\beta \\ r_{pf} &= r_{p0} + \Delta r_\alpha + \Delta r_\beta\end{aligned}$$

For the evolution of the orbital period and the final time we must take into account that the Sun-Earth perturbation does not increment the energy of the orbit (as it is shown in the semi major axis plot [Fig. 8]) so the period is kept constant with a reasonable accuracy.

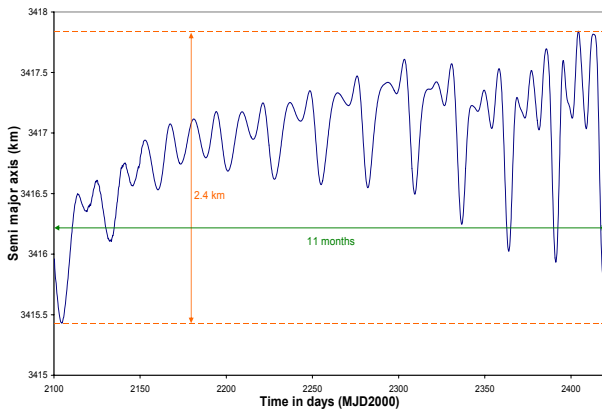


**Fig. 8:** Evolution of the semi major axis up to SMART-1 impact (without manoeuvres).

The equation for the final time is also more complex than the one of the final perilune radius, because the effect of the first will set the initial period for the second manoeuvre block. To pack the equation in a handy form we define the period at the end of each manoeuvre series as  $T_\alpha$  and  $T_\beta$  respectively

$$\left. \begin{aligned} T_\alpha &= T_0 + N_\alpha \cdot K_{2\alpha} \cdot \Delta V_\alpha \\ T_\beta &= T_\alpha + N_\beta \cdot K_{2\beta} \cdot \Delta V_\beta \end{aligned} \right\}$$

$$\left. \begin{aligned} \Delta T_\alpha &= N_\alpha \cdot T_0 + \frac{N_\alpha^2}{2} \cdot K_{2\alpha} \cdot \Delta V_\alpha \\ \Delta T_\beta &= N_\beta \cdot T_\alpha + \frac{N_\beta^2}{2} \cdot K_{2\beta} \cdot \Delta V_\beta \end{aligned} \right\}$$

$$t_f = t_0 + \Delta T_\alpha + L_\alpha \cdot T_\alpha + \Delta T_\beta + L_\beta \cdot T_\beta$$

## 6.2 Other constraints

Similar considerations for the illumination conditions and the visibility of the impact from Earth were made, to find initial values for the number of firing and free drift orbits N and L .

## 6.3 The final orbit

From the equation of the final time, we cannot fully deduce the impact time since in case the impact is missed a complete new orbit must be added. A similar problem occurs if the impact happens one orbit before. There is also an error of about 1 minute between the true impact time and the perilune time since the impact happens in the descending arc of the orbit and not exactly at perilune.

We can split the impact time variations in two parts of different magnitude: One big discrete correction of the order of an orbit period and a second one smaller and continuous of the order of the increment of period of a manoeuvre. For this second factor the following condition must be satisfied

$$N_\alpha + L_\alpha + N_\beta + L_\beta = const .$$

## 7. OPERATIONAL RESULTS

### 7.1 Iteration procedure

The algorithm to find an optimal solution is as follows:

- a) Choose  $N_\alpha$  and  $N_\beta$
- b) Obtain  $L_\alpha$  and  $L_\beta$  with the linear model using a default value for the impulses

- c) Implement a MANTRA case using these inputs. Set the optimisation constraints, including the height over the surface being greater than 0 for the last orbit and below 0 for the impact orbit.
- d) Run the case to obtain the manoeuvres magnitudes  $(\Delta V_\alpha, \Delta V_\beta)$  and the real impact time  $t_{\text{Impact}} = t(h = 0)$ .
- e) Analyze the results for feasibility and stability, which includes studying the magnitudes of the manoeuvres to be close to valid values and ensuring an impact point visible from Earth.

Once a first converged solution is found, one can transform it into initial conditions for further optimisations. This will result in shorter converging times.

The first iteration was done to select the impact coordinates. The criteria to accept a case was only the visibility from Earth and the duration of the thrust phase for each orbit. For performance reasons, the starting point of the first  $\Delta L$  must be below 120 degrees (measured in true anomaly from the apolune).

With this data, the scientific community selected an impact time between 5:30 and 6:30 UTC on the 3/9/2006 to be in the shadowed part of the Moon near the terminator, visible from La Silla (Chile).

The second iteration includes now the constraint for  $t_{\text{Impact}}$ . Several combinations of  $N_\alpha$  and  $N_\beta$  were studied to select the final scheme. The final strategy chosen had 67 orbits each with 7  $\Delta V_{\text{wol}}$  manoeuvres [Fig. 9/10]. It was split in 59 revolutions in June and 8 in July. For August a correction slot was reserved to correct for possible misperformances. Since in average no such deviations occurred, it was not needed.

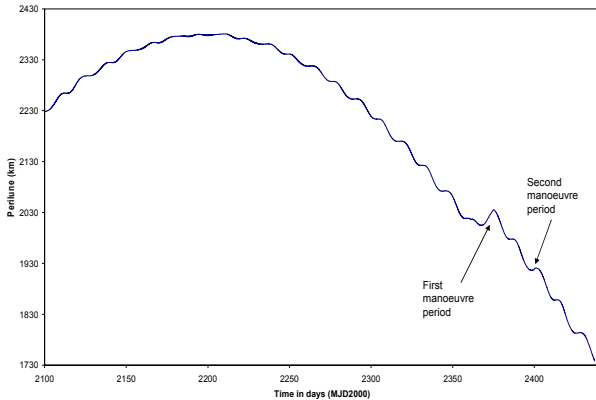


**Fig. 9:** Evolution of the perilune radius (with manoeuvres)

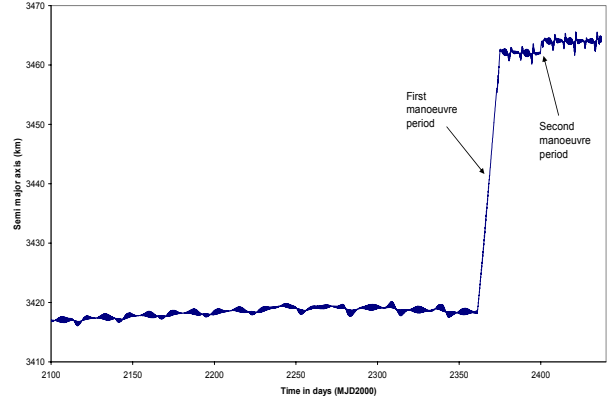


**Fig. 10:** Evolution of semi major axis (with manoeuvres)

## 7.2 Impulse magnitude adjustments

During operations, it is necessary to be able to adapt to the calibrated value of the manoeuvre performance. In order to quickly obtain a new approximation for the  $\Delta V_{\text{wol}}$  the following equations were used.

$$\left. \begin{aligned} r_{pf} &= r_{p0} + N \cdot M \cdot K_2 \cdot \Delta V_{\text{wol}} \\ r'_{pf} &= r_{p0} + N' \cdot M' \cdot K_2 \cdot \Delta V'_{\text{wol}} \end{aligned} \right\}$$

$$r_{pf} = r'_{pf} \Rightarrow \frac{N}{N'} \cdot \frac{M}{M'} \cdot \frac{\Delta V_{\text{wol}}}{\Delta V'_{\text{wol}}} = 1$$

Starting with N and M and keeping the final perilune radius but changing the number of impulses or the number of orbits one can determine new values (N' and M').

## 7.3 The Moon surface

We used the model W91 for the lunar surface. This model is available and was obtained from the Clementine NASA mission [9]. It has a distribution of mean heights in a 0.25x0.25 degrees grid in latitude and longitude over the reference ellipsoid. The deviation of this model from the real Moon surface and the effect of the gravity potential for very low orbits were the main uncertainties.

## 7.4 Last emergency manoeuvre

On the 31st of August, 3 days prior to the impact, Antony C. Cook suggested a more accurate surface model. An analysis of the last orbit determination with this new model showed that the probability of hitting the edge of the Clausius crater one orbit before the predicted impact was too high [Fig. 11].

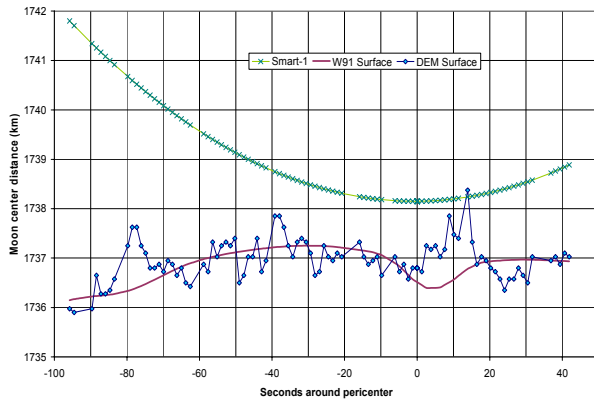


**Fig. 11:** Study of the last orbit with the more accurate Antony C. Cook surface model [10].

To avoid the collision risk in an earlier orbit a correction manoeuvre was performed, to raise the perilune by 600 meters. This ensured the S/C to be above the uncertainty in height of the A. C. Cook model. The nominal impact

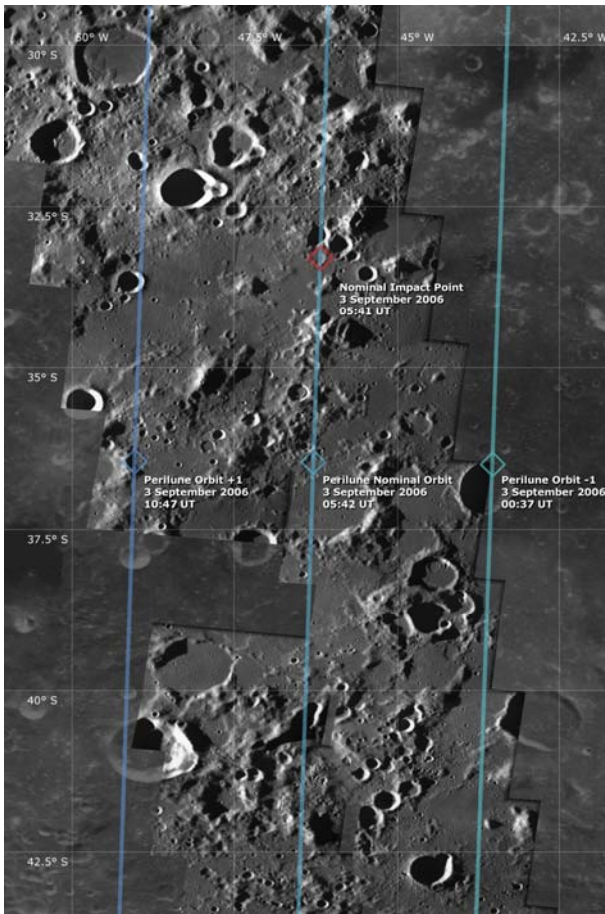


**Fig. 12:** Mosaic of images of the SMART-1 impact site, obtained by the Advanced Moon Imaging Experiment (AMIE) on board SMART-1, Mark R. Rosiek [11].

was still met, since SMART-1 lost 1200 Meter of height per orbit. On the 1/9/2006 a Safe Mode occurred just before the new profile with the emergency manoeuvre

could be up linked. Thanks to the effort and experience of the operation team, the satellite could be recovered quickly and updated commands were up linked.

## 8. CONCLUSION

Using the on-board control logic, which converts a  $\Delta L$  manoeuvre into a  $\Delta V$ , and a flexible attitude generator the equivalent to a proper low thrust motor could be provided. The optimisation was based on the same software and similar ideas as for the earlier EP-firing phases. Clear interfaces in-between these two tasks were helpful to cut down the overall complexity. Although the feasibility was completely unknown at the time of the initial planning and many concerns arose, the final implementation proved to be very stable and smooth. Already with the first manoeuvre sequence sufficient accuracy was achieved, i.e. no further detailed refinement of the procedure was required, apart from standard calibrations. The science community was awaiting the impact on the morning of 3/9/2007. At 5:42:21.759 UTC the SMART-1 carrier signal dropped to zero and the CFHT (Canada-France-Hawaii Telescope) infrared telescope recorded a flair at exactly the expected impact point (46.20W 43.44S) [Fig. 12].

## References

- 1 SMART-1 A Solar-Powered Visit to the Moon. ESA bulletin No. 113, February 2003
- 2 SMART-1 Operational pointing Constraints, Per Bodin, Swedish Space Cooperation, Technical Note S1-AOCS-TN-45, June 16, 2004
- 3 SMART-1 Impact predictions and observation campaign, B.H. Foing et al, revised 29 August 2006
- 4 The Optimisation of Attitude Profiles for SMART-1 : A Highly Constraint Problem, R. Rigger, J.J. Yde, M. Mueller & V. Companys. 18<sup>th</sup> International Symposium on Space Flight Dynamics 2004.
- 5 SMART-1 AOCS End of Mission Analysis, Per Bodin, Swedish Space Cooperation, Report S1-SSC-RP-2325, May 4, 2006.
- 6 Graphic by Juurian De Bruin, 2006 (SMART-1 FCT).
- 7 SMART-1 End-of-mission planning, J. Schoen-maekers, A. Ayala, R. Rigger, ESOC/FD, Issue 1, 7 March 2006
- 8 An Introduction to the Mathematics and Methods of Astrodynamics, Richard H. Battin AIAA Education Series 1987
- 9 PDS NASA repository for Clementine, <http://pds-geosciences.wustl.edu/missions/clementine/>
- 10 Antony C. Cook, <http://www.cs.nott.ac.uk/~acc/>
- 11 Photo: ESA/Space-X (Space Exploration Institute), <http://astrogeology.usgs.gov/Teams/Geomatics/>, Mark R. Rosiek